Direct Numerical Simulation of Mixing and Chemical Reactions in a Round Jet into a Crossflow - a Benchmark

J.A. Denev[1], J. Fröhlich[1] and H. Bockhorn[1]

1 Institute for Technical Chemistry and Polymer Chemistry
{denev,froehlich,bockhorn}@ict.uni-karlsruhe.de

Abstract

A benchmark simulation of the jet in crossflow (JICF) configuration is presented in detail. A Direct Numerical Simulation (DNS) was carried out with a low Reynolds number equal to 275 and a jet-to-crossflow velocity ratio equal to 2.4. The benchmark is carefully selected to provide reference data concerning the following phenomena: the flowfield, the mixing process of passive scalars and three chemical reactions. The data presented concern both instantaneous and time-averaged values as well as the corresponding fluctuations. To facilitate the quantitative comparison with the data from the present work various one-dimensional plots are presented. To allow easy repetition of the present numerical benchmark, both the jet and the crossflow are supplied at laminar flow conditions. As a result of this a transition zone occurs which in turn constitutes a severe test for any simulation methodology.

1 Introduction

The present investigation is part of the Priority Programme SPP-1141 "Analysis, modeling and computation of flow mixing apparatus with and without chemical reactions" of the German Research Foundation (DFG). The overall goal of this programme is to develop analytical and numerical methods for the reliable prediction of flow and concentration fields in mixings devices, including chemical reactions. To achieve this, a detailed understanding of the flow physics is necessary. With this purpose a Direct Numerical Simulation (DNS) of a jet in crossflow is carried out in the present investigation. The careful selection of both the flow and the numerical parameters targets the development of a suitable benchmark configuration for the JICF.

The specification of a benchmark configuration is a delicate issue. On one hand, it has to represent a physically meaningful and challenging test for the

models to be scrutinized. On the other hand, it must be simple enough to allow unambiguous specification of all conditions.

Since the specification of turbulent inflow conditions for DNS and Large Eddy Simulations (LES) is a delicate task which often inhibits close comparison between different simulations, it was decided to devise a case with entirely laminar inflow conditions. Thus the use of a precursor simulation for generation of unsteady turbulent inflow data is avoided and only the time-average shape of the inflow profile has to be specified in the simulation. In accordance to the previous experience of the authors [6], [4], up to 25% of the CPU-Time for LES and DNS could be saved when such precursor simulations are dropped. At the same time, the laminar inflow conditions lead to the presence of a transition zone in the flow, thus presenting a hard test for statistical turbulence models for RANS (Reynolds Averaged Navier Stokes) simulations or subgrid models for LES.

DNS benchmarks exist for many other flow types, but the complex geometry prevents most of the spectral-based codes from simulating the complete JICF configuration. Just recently increasing computer power allowed finite volume codes to meet the challenges of DNS simulations of the JICF. In their DNS Hahn and Choi [8] make use of a Carthesian grid and simulate only the crossflow. The effect of the round pipe has been accounted for by specifying a parabolic profile at the bottom wall of the domain. In their study the jet-to-crossflow velocity ratio $R = U_{jet}/U_{crossflow}$ was set to 0.5 to examine a film cooling configuration. The Reynolds number throughout this paper is defined with the jet-diameter and the velocity of the crossflow, $Re = U_\infty D/\nu$, where ν is the kinematic viscosity.

Sharma and Acharya [15] simulate a configuration with $R = 0.25$ and a rectangular jet relevant to film cooling of gas turbine blades and combustor walls. Muldoon [10], [1] presents DNS results of pulsating jets to study the effect of the Strouhal number and the waveforms on the flow structures and the mixing of a JICF. The investigations of Muppidi and Mahesh [13, 11, 14] follow the experiments of Su and Mungal [16] and use a relative high velocity ratio $R = 5.7$. In order to specify the boundary conditions in the pipe, a separate simulation of a fully turbulent pipe flow has been conducted. The data from a plane of this separate simulation have been stored and interpolated at the pipe inflow (pipe length equal to two diameters) thus making any repetition of the simulation by others quite difficult. In [12] the same authors present results only for the jet trajectories. However, in this study they use a different approach for the boundary conditions. They specify a "parabolic" and a "mean-turbulent" profile at the entrance of the pipe (10 diameters long) and do not report using any turbulence-generating approach for the different flow configurations with pipe-Reynolds numbers $Re = 1500, R = 1.5$ and $Re = 5000, R = 5.7$.

Unlike previous numerical investigations, the present work uses a set of well-specified laminar boundary conditions for both, the pipe and the crossflow which are easy to impose in any numerical code. To support further the

target of benchmarking, quantitative results are presented for a wide range of phenomena: fluid flow and its coherent structures, mixing of passive scalars and simple chemical reactions. The jet-to-crossflow velocity ratio $R = 2.42$ used in the present study specifies a jet trajectory which is away from any adjacent channel wall.

2 The flow configuration and the boundary conditions

In a companion project at the same institute experimental work is currently performed for the same configuration [17]. These measurements have not yet been terminated, but the geometry of the flow and some of the boundary conditions are selected according to the experimental setup to support future data validation. The flow configuration is shown in Fig. 1 together with the employed coordinate system. All lengths are made dimensionless with the reference value being the jet diameter ($D = 8\ mm$ in the experiment): $L_x = 20$, $L_y = L_z = 13.5$, $l_x = 3$ and $l_z = 2$. The reference velocity $U = U_\infty = U_{crossflow} = U_{max}$ is the velocity of the crossflow at the middle of the main channel which appears to be the maximum velocity (and not the bulk velocity) of the channel. The most important physical parameters for this flow are the Reynolds number and the velocity ratio between jet and crossflow. The latter is defined here with the bulk velocity of the jet ($U_{b,jet}$), i.e. $R = U_{b,jet}/U$. Its value in the present case is $R = 2.42$ and has been selected to obtain a location of the jet remote from the channel walls. The Reynolds number based on the bulk velocity in the pipe hence is $Re_{jet} = U_{b,jet}D/\nu = 666$ so that both, crossflow and pipe flow appear laminar.

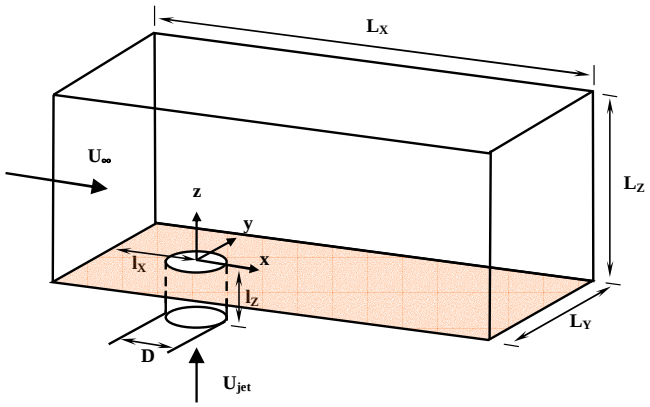

Fig. 1. The flow configuration.

In the simulation a parabolic velocity profile:

$$w(r)/U_{b,jet} = 2[1 - (r/(D/2)^2] \tag{1}$$

was imposed at the origin of the pipe. Here, r is the radial coordinate and w the vertical velocity component. With the kinematic viscosity of air $\nu = 1.406 \times 10^{-05}\ m^2/s$ the dimensional bulk velocity of the jet corresponds to $U_{b,jet} = 1.16\ m/s$. This boundary condition is shown together with the resulted profile at the end of the pipe (at $y/D = 0$) in Fig. 2. The profile at $z/D = -1.0$ (not shown) is practically the same as the boundary condition, i.e. unaffected from the crossflow.

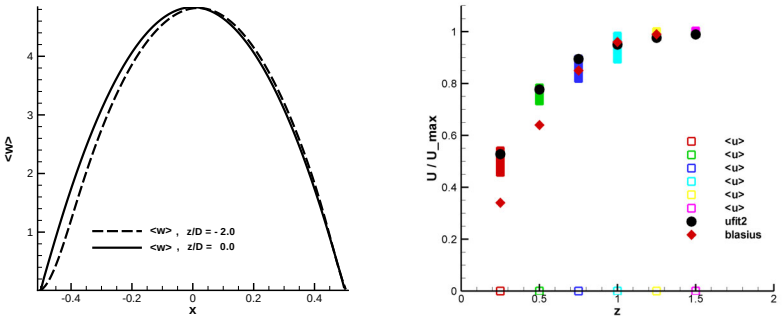

Fig. 2. Left: The profile in the pipe at $z/D = -2.0$ used as boundary condition and at the jet entrance, $z/D = 0.0$. Right: The experimentally measured velocities, the Blasius profile and the curve fit used in the simulation.

The low Reynolds number creates a relatively large boundary layer along the walls of the duct. The shape of the boundary layer along the bottom wall is given in Fig. 2. The squares represent the measured data (PIV without the jet flow, planes $z = const$) at different distances from the bottom wall. The circles show the fit to these data used in the simulation, yielding a boundary layer thickness $\delta_{99\%} = 1.54D$. A Blasius profile with the same thickness is also shown for comparison. The boundary layer was not explicitly measured at the other walls, but for reasons of symmetry the same boundary layer shape was assumed in the simulation so that the u-velocity component at the inflow boundary has been defined by:

$$u(d_n) = 1.0 - \exp(-3.0\ d_n) \quad , \tag{2}$$

where d_n is the normal distance to the closest channel wall. The two other velocity components (v, w) are set to zero at the inflow boundary. Equation (2) yields $U_{max} = 1.0$ in the middle of the channel and $U_b/U_{max} = 0.905$, where U_b is the bulk velocity in the channel. A convective outflow boundary condition is used at the channel exit. For all walls no-slip boundary conditions are applied.

Apart from the velocity field, the transport of seven scalar variables have been calculated. These do not influence the density and hence are passive scalars for the flow field. The transport of all scalars can therefore be computed in the same simulation without mutual interaction. The first scalar is non-reactive and introduced with the jet where its value is set to 1 while being 0 in the crossflow. Its Schmidt number $Sc_1 = 0.96$ has been selected to match the diffusion of NO_2 in air which is the non-reacting tracer in the experiment. The remaining six scalars are reactive. Variations of Schmidt and Damköhler number have been performed as detailed in Table1 in order to investigate their respective influence. Three model reactions of type $A + B \rightarrow P$ are considered in the study with reaction rate $\omega_{A,B} = Da_{A,B} Y_A Y_B$ where Y_A and Y_B are the mass concentration of the species A and B, respectively. Since Y_A, Y_B and Y_P sum up to unity, the concentration of the product Y_P needs not be computed. The scalars in column A of Tab. 1 are introduced with the jet while those of column B have concentration 1 in the crossflow and 0 in the jet. The Damköhler number Da characterizes the ratio of the characteristic flow time to the characteristic chemical reaction time. Hence, large values correspond to fast combustion occurring in very thin layers requiring a correspondingly fine numerical grid to resolve these reaction fronts. The values of Da have been selected here such that the cost of the simulation remains within the available limits.

Table 1. Schmidt and Damköhler numbers used in the present study.

	A	B	Da
No reaction:	$Sc_1 = 0.96$		
Reaction 1:	$Sc_2 = 1.0$	$Sc_3 = 1.0$	$Da_{2,3} = 1.0$
Reaction 2:	$Sc_4 = 1.0$	$Sc_5 = 1.0$	$Da_{4,5} = 0.5$
Reaction 3:	$Sc_6 = 2.0$	$Sc_7 = 1.0$	$Da_{6,7} = 1.0$

3 Numerical method

The Finite Volume code LESOCC2 (Large Eddy Simulation On Curvilinear Coordinates, version 2) [9] has been used in the present simulations. It solves the incompressible Navier-Stokes equations using second order central differences for the convective and the viscous fluxes together with the Rhie-Chow momentum interpolation on collocated grids. A three-step low-storage Runge-Kutta method is used for time-advancement. A Poisson-type equation is solved for the pressure-correction using the Strongly Implicit Procedure Procedure (SIP). The code uses body-fitted curvilinear block-structured grids and information between processors is exchanged via MPI.

If block-structured grids allow only matching cells at block boundaries, the overall number of control volumes increases quickly when the mesh is refined in any area of the computational domain. To overcome this, a local grid refinement technique has been implemented recently in the code. It allows local refinement of blocks by integer fractions compared to neighbouring block. As shown below, this can be used to improve the distribution of control volumes within the computational domain. The local refinement technique has been tested prior to this investigation on a Taylor-vortex and channel flows and data from the latter have been reported in [7].

4 Details of the numerical grid and parallelization

The present grid containing 22.3 Mio cells has been generated with ICEM-CFD v4.3.3. It is partitioned into 219 numerical blocks. Out of these, 42 are locally refined in all three spatial directions by a factor of 3 as displayed in Fig. 3. The refined blocks are located close to the jet exit where gradients are large and transition takes place. The location of refinement was chosen after a preliminary simulation on a coarser grid. Despite the fact, that the refined blocks only cover a small portion of the computational domain, they contain 89% of the cells. Load balancing was obtained by an evolutionary algorithm based on the number of cells per processor. An optimal distribution was obtained with 31 or 32 processors. With 31 processors of the HP XC6000 Cluster at the Computer Centre Karlsruhe this yielded an average "user time" of 90.97% while the communication required was 9.03% (Overhead: 8.46%; Blocking: 0.57%).

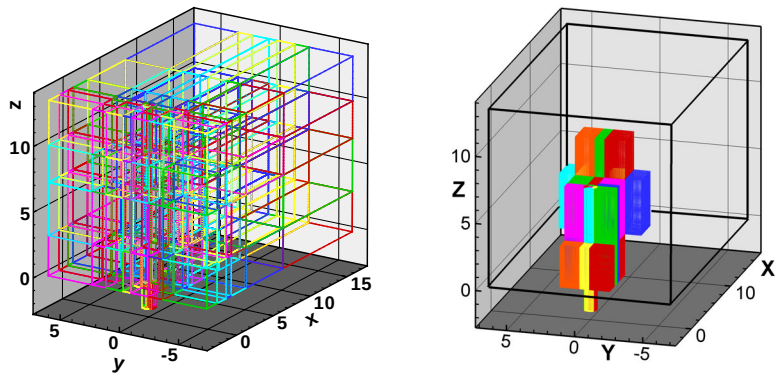

Fig. 3. Block boundaries of all 219 blocks of the grid (left) and overview of the refined blocks near the jet-exit (right).

An O-grid topology was used in the pipe containing 144 almost equally distributed points along the pipe diameter. In vertical direction the pipe con-

tains 60 gridpoints. Their size Δz is equally decreasing toward the pipe exit, where it reaches the value $\Delta z = 0.026D$. Thirty-three points are located in the $\delta_{99\%}$ boundary layer of the bottom wall of the crossflow channel. The resolution capacity of the grid was assessed in physical terms by evaluating an LES subgrid-scale model during one time step of the developed solution. For a true DNS its contribution should be very small. In the present case, the Smagorinsky model with the standard choice of $C_s = 0.1$ for the constant involved in this model yielded an eddy viscosity below 3% of the molecular viscosity in the refined blocks as illustrated in Fig. 4. Bearing in mind that this model yields a turbulent viscosity even in the laminar case, this shows the resolution to be adequate for a DNS with the present grid.

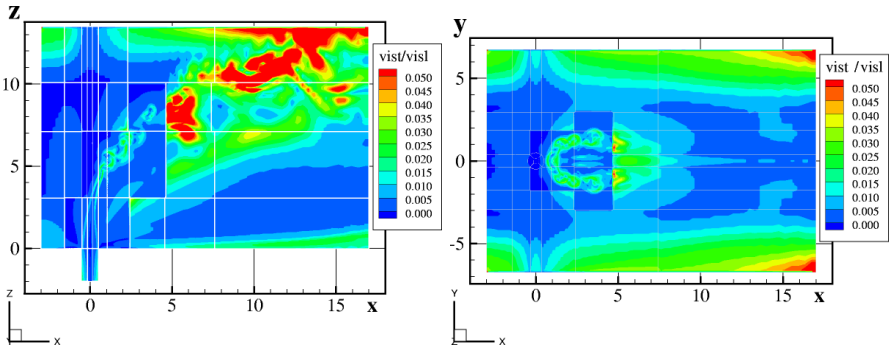

Fig. 4. The ratio of turbulent viscosity to molecular viscosity obtained with the Smagorinsky model for one iteration, planes $y = 0$ and $z/D = 5$.

5 Results

All figures below, including representations of the grid, have been obtained by consideration of every second cell in the full computational grid.

5.1 Statistical data

The unsteady flow was computed over an initial period of 60 time units D/U before statistical averaging was started. The averaging has been performed over 50 time units.

The CFL number has to be restricted due to the explicit time integration scheme and for physical reasons, to resolve the flow in time. Its value for the present computation is CFL=0.96 yielding a dimensionless time step of 0.00082. The timestep was set constant in view of the Fourier and wavelet analyses for the timesignals to be made at a later stage.

5.2 Instantaneous data and flow structures

A first evaluation of the flow structures is based on the three dimensional pressure field. An iso-surface of the instantaneous pressure fluctuation which allows the visualization of the large vortex structures is plotted in Fig. 5. A companion visualization by the Q-criterion [5] is provided as well. These pictures show three types of structures: the boundary of the jet close to the outlet, spanwise rollers on the upper surface of the jet and further downstream two vortices aligned with the axis of the jet, the so-called counter-rotating vortex pair (CVP). The vortices shown are typical for the jet in crossflow configuration. Unlike previous simulations of the authors [6, 4] performed at higher Re with a turbulent jet-pipe flow, the present flow structures are clear cut and easier to identify due to the low Reynolds number.

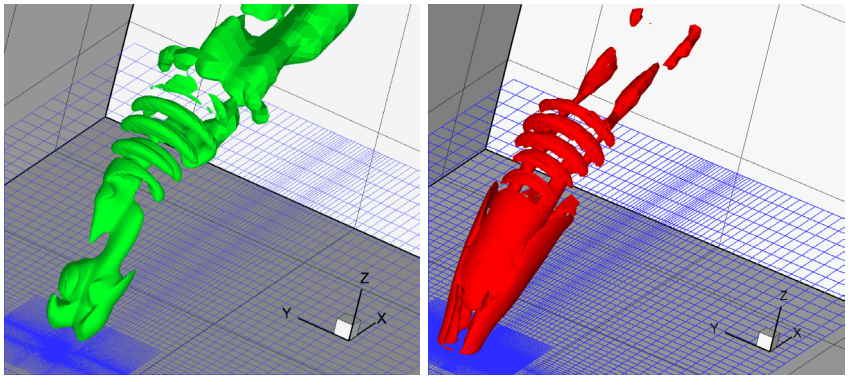

Fig. 5. Left: Coherent structures of the flow visualized by the isosurface $p - p_{average} = -0.035$. Right: The same structures visualized by the Q-criterion, $Q = 1.6$.

Instantaneous plots of the non-reactive scalar S_1 and the reactive scalar S_2 originating in the jet (see Table 1) are presented in Fig. 6 for the centerplane $y = 0.0$. Both plots are taken at the same time at which the jet trajectory is also shown. Subsequent plots of the concentration field reveal that the position of the transition point changes with time. The position of the transition point has been found to vary between $x/D = 2.0$ and $x/D = 3.0$ for the different times plotted, which corresponds to a path of $s = 4.8D$ to $s = 6.0D$ along the jet trajectory, respectively. Those values, defined here as the position of the first waves, appearing near the jet-trajectory in the level-plots of scalar S_1 (see Fig. 6), correspond well with the the experimental data of [2].

5.3 Statistical data in the centerplane

Fig. 7 shows the jet trajectory in the centerplane, determined by the stream-trace of the time-averaged velocity field, which originates at the middle of

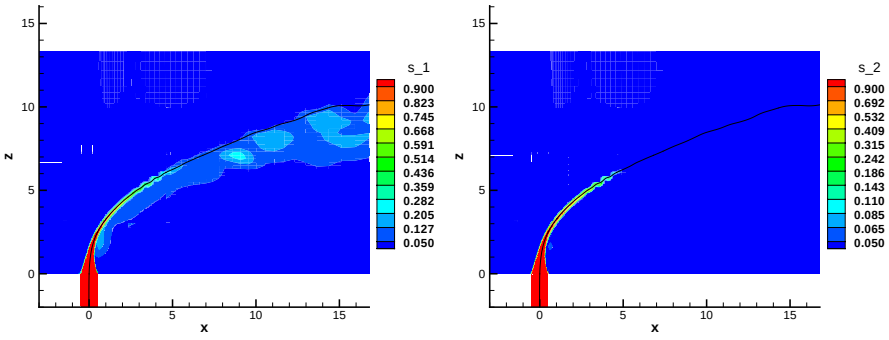

Fig. 6. The concentration of S_1 (left) and S_2 (right) in the symmetry plane.

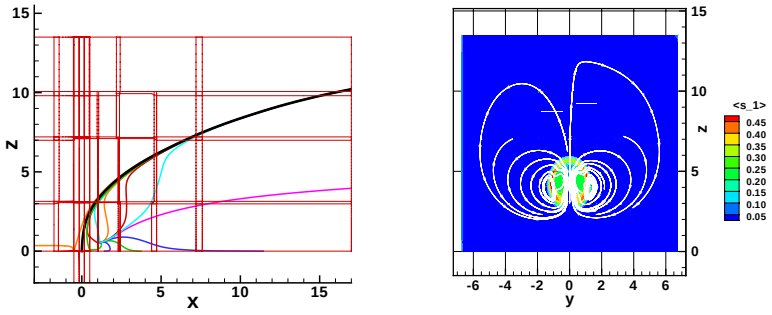

Fig. 7. Streamtraces of the averaged flow in the centerplane and distribution of the averaged scalar concentration $\langle S_1 \rangle$ at $x/D = 4.0$.

the pipe-exit $(x, y, z = 0)$. Furthermore, selected streamlines are visualized which demonstrate the complicated flow patterns behind the jet with locally reverse and locally descending flow. The saddle point in this graph, where all streamtraces originate, is located at $(x/D, z/D) = (1.16, 0.55)$. The near-bottom streamtrace at the left hand side of the jet shows that, similar to the case with R=5.7 of [12], there exists no hovering vortex near the pipe-end, which is due to the relative strong jet momentum investigated.

The contour plot on the right hand side of Fig. 7 shows the scalar concentration at $x/D = 4.0$ together with the streamtraces in that plane. The counter-rotating vortices are clearly seen together with the upward flow of ambient fluid in the middle of the jet. This upward flow is in accordance with the streamtraces on the left picture of Fig. 7. It is the main reason for the good mixing properties of the JICF configuration as shown also by the mixing indices studied in [3].

Figures 8-12 show quantitative data for means and fluctuations along vertical cuts in the centerplane. The axial positions have been normalized by RD and correspond to $x/D = 0.0$, $x/D = 1.45$, $x/D = 2.90$ and $x/D = 4.35$, respectively. In Fig. 8 the negative $\langle u \rangle$-component is clearly apparent together with negative values of $\langle w \rangle$ near the bottom. The position of the jet is related to narrow peaks in both components. The corresponding fluctuations in Fig. 9 also exhibit peaks at these positions while their level remote from the jet is very low. An exception is w_{RMS} at $x/RD = 0.6$.

Fig. 10 displays the four scalars introduced with the jet, S_1 being the non-reactive, while the other three are described in Table 1. It is apparent that the reactive scalars are consumed and hence attain a lower level downstream. The differences in Da and Sc, on the other hand, are not large enough to induce substantial differences, although the peak of S_2 at $x/(RD) = 1.8$ is only two thirds of the maximum of $\langle S_4 \rangle$. Due to the reaction, the CVP does not manage to increase the level of $\langle S_2 \rangle$, $\langle S_4 \rangle$ and $\langle S_6 \rangle$ below the trajectory since the scalars are consumed on their way. This is different with the non-reactive scalar $\langle S_1 \rangle$ which has a value of about one thirds the peak level just below the jet at $x/(RD) = 1.8$.

The RMS-values of S_1 are given in Fig. 11. They exhibit a double peak in the jet and small values below the jet, for the reasons explained above. Fig. 12 shows the three reaction rates and illustrates the consumption in and below the jet. Fig. 13 finally provides the turbulent fluxes of S_1 in streamwise and vertical direction. Apart from $x = 0$ where the jet is vertical, they both have about the same level. A particularity is the negative peak of $\langle w' s_1' \rangle$ at the right-most position.

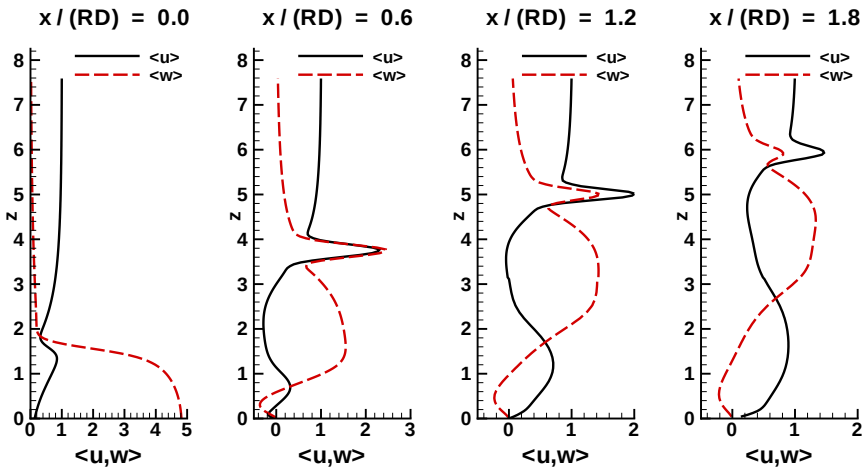

Fig. 8. Mean velocity $\langle u \rangle$ and $\langle w \rangle$ in the centerplane.

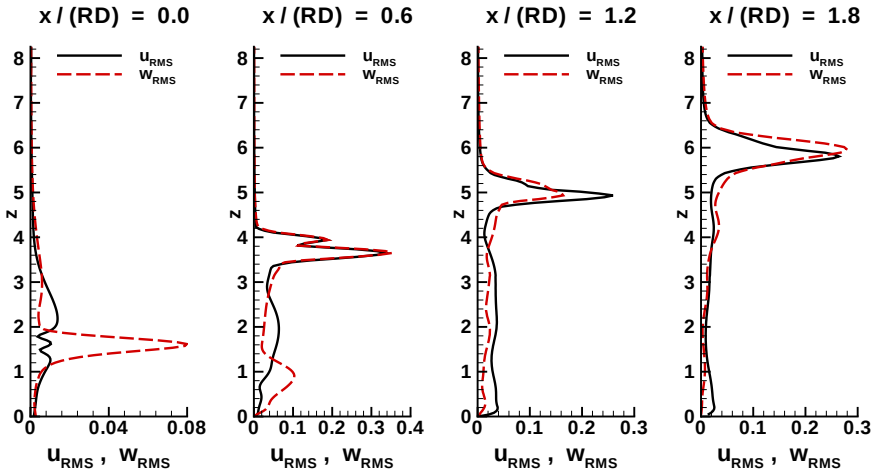

Fig. 9. Velocity fluctuations (RMS) in the centerplane.

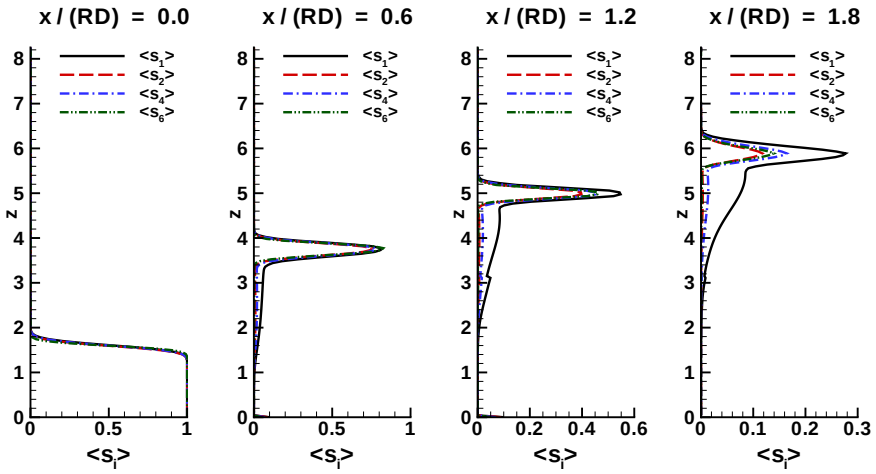

Fig. 10. Mean scalar concentrations in the centerplane.

5.4 Computational resources

The computation was performed on 31 processors of the HP XC6000 Cluster of the Computer Centre at the University of Karlsruhe. In total 110 dimensionless time units D/U were calculated. Each dimensionless time unit consists of 1220 time steps and requires $21.3h$ CPU-Time (on 31 processors). The computation of the seven scalar variables with the three chemical reactions takes approximately 54% of the total CPU-time, 46% are spent for the velocity field, mainly for the pressure-correction which results from the solution of a Poisson

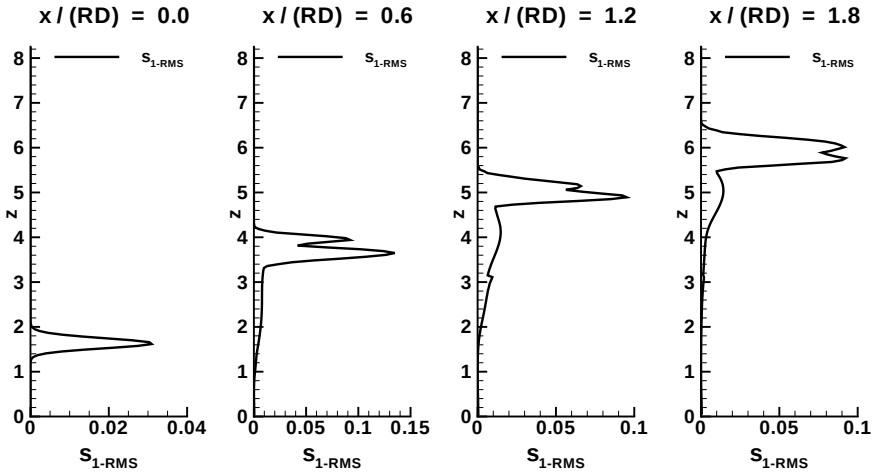

Fig. 11. RMS-fluctuations of the non-reactive scalar S_1 in the centerplane.

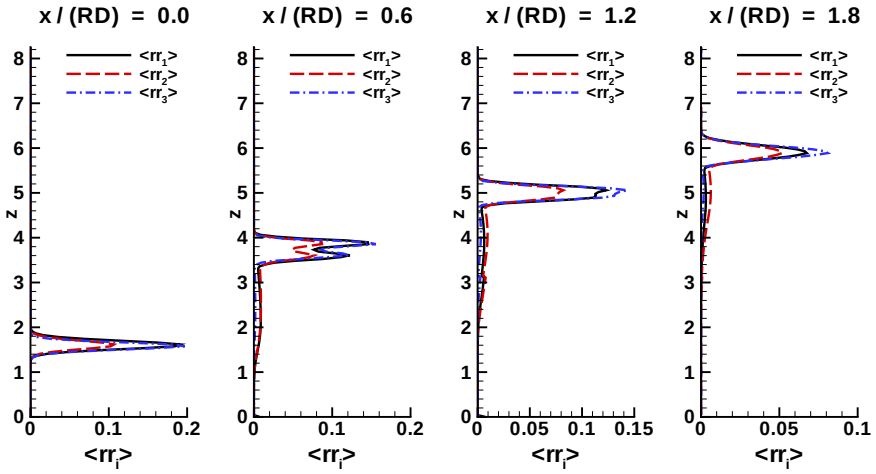

Fig. 12. Reaction rate of reactions 1-3 in Table 1.

equation. The required RAM is below 1Gb per processor. The disk space to store the compressed (zipped) binary data containing both instantaneous and averaged values is 4,6 GB. Another 10 GB are required for postprocessing these data.

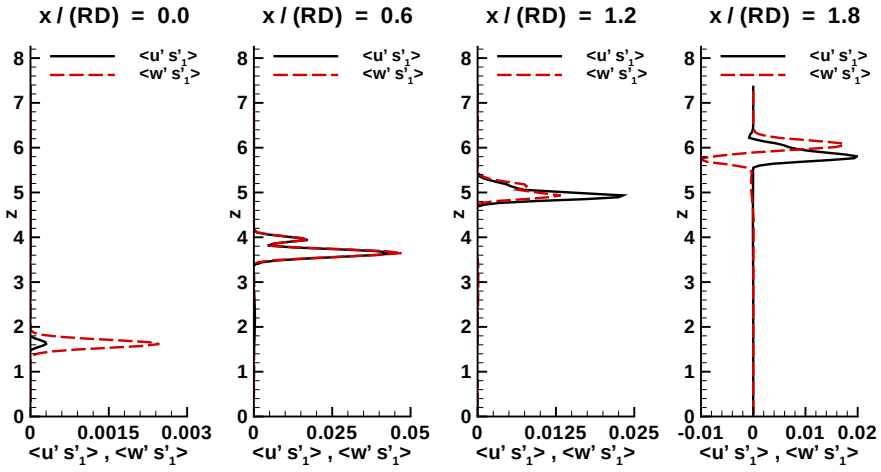

Fig. 13. Turbulent fluxes of the non-reactive scalar in streamwise and vertical direction, $\langle u's_1' \rangle$ and $\langle w's_1' \rangle$, respectively.

6 Conclusions

Direct numerical simulations are exempt from any turbulence model and can hence provide reference data for the calibration and validation of LES (Large Eddy Simulation) subbgrid models or turbulent models for RANS (Reynolds Averaged Navier Stokes equations) simulations. The present computations were devised to serve as a benchmark of the jet in crossflow configuration at low Reynolds numbers. For this purpose the physical and numerical parameters have been adjusted to yield a compromise between diverging requirements:

- simplifying the numerical efforts and decreasing the numerical uncertainty by imposing laminar boundary conditions in both the jet and the crossflow;
- specifying values for the Reynolds number and the velocity ratio R which yield a jet trajectory away of the channel walls;
- specifying values for the Reynolds number and the velocity ratio R to obtain a possibly short transition length of the jet - in order to decrease the region with fine grid and to keep numerical resources bounded.

The last requirement was not fully met in the present investigation and a transition has been found to occur approximately $5-6$ diameters downstream the jet trajectory, varying with the time. However, the fact that a large area of the computational domain is still laminar, allows the present data to be compared also with coarse-grid DNS.

Detailed description of the present boundary conditions aims at easy comparison of the present data with the results of other numerical groups. This

target is supported also by the various one-dimensional plots of averaged and fluctuating quantities presented.

A further feature of the present benchmark is the presentation of data regarding also mixing of passive scalars and simple chemical reactions with different values of the Schmidt and Damköhler numbers.

After publishing the results, the data from the one-dimensional plots will be made available for comparison at:
http://www.ict.uni-karlsruhe.de/ index.pl/themen/dns/index.html.

Acknowledgements

The authors gratefully acknowledge funding by the DFG through SPP 1141 and provision of computing time at the Karlsruhe Supercomputer Center. The authors would like to thank their colleagues Priv. Doz. Dr. habil. Rainer Suntz and Dipl.-Ing. Camilo Cardenas for delivering the data for the boundary layer of the crossflow.

References

1. $url = www.navo.hpc.mil/Navigator/sp04\_Feature3.html$.
2. R. Camussi, G.Guj, and A. Stella. Experimental study of a jet in a crossflow at very low reynolds number. *J. Fluid Mech.*, 454:113–144, 2002.
3. J.A. Denev, J. Fröhlich, and H. Bockhorn. Evaluation of mixing and chemical reactions within a jet in crossflow by means of LES. In *Proc. European Combustion Meeting, April 3–6, Louvain, Belgium, 2005*, pages CD–ROM, Louvain-la-Neuve, Belgium, 2005. Université Catholique de Louvain.
4. J.A. Denev, J. Fröhlich, and H. Bockhorn. Structure and mixing of a swirling transverse jet into a crossflow. In J.A.C. Humphrey, T.B. Gatski, J.K. Eaton, R. Friedrich, N. Kasagi, and M.A. Leschziner, editors, *Proceedings of 4th Int. Symp. on Turbulence and Shear Flow Phenomena, June 27–29 2005, Williamsburg, Virginia*, pages 1255–1260, 2005.
5. Y. Dubief and F. Delcayre. On coherent-vortex identification in turbulence. *J. Turbulence*, 1(11), 2000.
6. J. Fröhlich, J.A. Denev, and H. Bockhorn. Large eddy simulation of a jet in crossflow. In *Proceedings of ECCOMAS 2004, Jyväskylä, Finland, July 24-28, ISBN 951-39-1868-8, CD-ROM*, Barcelona, 2004. CIMNE.
7. J. Fröhlich, J.A. Denev, C. Hinterberger, and H. Bockhorn. On the impact of tangential grid refinement on subgrid-scale modelling in large eddy simulations. In *Sixth International Conference on Numerical Methods and Applications - NM&A'06 August 20–24, 2006, Borovets, Bulgaria*, 2006.
8. S. Hahn and H. Choi. Unsteady simulation of jets in a cross flow. *J. Comput. Phys.*, 134:342–356, 1997.
9. C. Hinterberger. *Dreidimensionale und tiefengemittelte Large–Eddy–Simulation von Flachwasserströmungen*. PhD thesis, Institute for Hydromechanics, University of Karlsruhe, http://www.uvka.de/univerlag/volltexte/2004/25/, 2004.

10. F. Muldoon. *Numerical Methods for the Unsteady Incompressible Navier-Stokes Equations and Their Application to the Direct Numerical Simulation of Turbulent Flows*. PhD thesis, Louisiana State University, 2004.
11. S. Muppidi and K. Mahesh. Direct numerical simulation of turbulent jets in crossflow. In *43 rd AIAA Aerospace Sciences Meeting and Exibit*, Reno, Nevada, Jan 10-13 2005. AIAA Paper 2005-1115.
12. S. Muppidi and K. Mahesh. Study of trajectories of jets in crossflow using direct numerical simulations. *J. Fluid Mech.*, 530:81–100, 2005.
13. S. Muppidi and K. Mahesh. Velocity field of a round turbulent transverse jet. In J.A.C. Humphrey, T.B. Gatski, J.K. Eaton, R. Friedrich, N. Kasagi, and M.A. Leschziner, editors, *Fourth International Symposium. on Turbulence and Shear Flow Phenomena*, Paper TSFP4-197, pages 829–833, Williamsburg, Virginia, 2005.
14. S. Muppidi and K. Mahesh. Passive scalar mixing in jets in crossflow. In *44th AIAA Aerospace Sciences Meeting and Exhibit*, Reno, Nevada, Jan 9-12 2006. AIAA Paper 2006-1098.
15. Ch. Sharma and S. Acharya. Direct numerical simulation of a coolant jet in a periodic crossflow. Technical report, National Aeronautics and Space Adminisatration, October 1998.
16. L. K. Su and M. G. Mungal. Simultaneous measurements of scalar and velocity field evolution in turbulent crossflowing jets. *J. Fluid Mech.*, 513:1–45, 2004.
17. R. Suntz and C. Cardenas. Analysis, modeling and computation of flow mixing aparatus with and wihtout chemical reactions. Technical report, DFG-Report, Priority Programme SPP-1141, June 2006.